Modeling Assisted Room Temperature Operation of Atomic Precision Advanced Manufacturing Devices

Xujiao Gao
Electrical Models & Simulation
Sandia National Laboratories
Albuquerque, USA
xngao@sandia.gov

Lisa Tracy
Quantum Phenomena
Sandia National Laboratories
Albuquerque, USA
latracy@sandia.gov

Evan Anderson
Multiscale Fab Sci & Tech Dev
Sandia National Laboratories
Albuquerque, USA
emander@sandia.gov

DeAnna Campbell
Biological & Chemical Sensors
Sandia National Laboratories
Albuquerque, USA
dmlope@sandia.gov

Jeffrey Ivie
Multiscale Fab Sci & Tech Dev
Sandia National Laboratories
Albuquerque, USA
jaivie@sandia.gov

Tzu-Ming Lu
Quantum Phenomena
Sandia National Laboratories
Albuquerque, USA
tlu@sandia.gov

Denis Mamaluy
Cognitive & Emerging Computing
Sandia National Laboratories
Albuquerque, USA
dnmamal@sandia.gov

Scott Schmuckery
Multiscale Fab Sci & Tech Dev
Sandia National Laboratories
Albuquerque, USA
swschmu@sandia.gov

Shashank Misra
Multiscale Fab Sci & Tech Dev
Sandia National Laboratories
Albuquerque, USA
smisra@sandia.gov

***Abstract*—One big challenge of the emerging atomic precision advanced manufacturing (APAM) technology for microelectronics application is to realize APAM devices that operate at room temperature (RT). We demonstrate that semiclassical technology computer aided design (TCAD) device simulation tool can be employed to understand current leakage and improve APAM device design for RT operation. To establish the applicability of semiclassical simulation, we first show that a semiclassical impurity scattering model with the Fermi-Dirac statistics can explain the very low mobility in APAM devices quite well; we also show semiclassical TCAD reproduces measured sheet resistances when proper mobility values are used. We then apply semiclassical TCAD to simulate current leakage in realistic APAM wires. With insights from modeling, we were able to improve device design, fabricate Hall bars, and demonstrate RT operation for the very first time.**

Keywords—atomic precision advanced manufacturing (APAM), room temperature operation, current leakage, semiclassical TCAD, ionized impurity scattering

I. Introduction

Atomic Precision Advanced Manufacturing (APAM) is a process of area-selective chemical incorporation of dopants at an atomic scale using the scanning tunneling microscope (STM) technique [1]. Expanding what APAM can do unlocks the door to revolutionary opportunities in microelectronics from the very physical limit of atoms [2]. Current APAM devices can only work at cryogenic temperatures which is sufficient for quantum computing applications [3]. However, to make any potential impact to microelectronics, APAM devices must work at room temperature (RT). To address this challenge, an interdisciplinary experimental and modeling team at Sandia National Laboratories work closely together to enable APAM devices towards RT operation.

A typical APAM wire designed to operate at cryogenic temperatures is schematically shown in Fig. 1, where a phosphorous (P)-doped delta-layer using STM is capped by a silicon epitaxy layer to activate the P dopants and is contacted to heavily doped implant regions. The leakage paths through the substrate and cap layers are freeze-out at 4 Kelvin, but they become important at RT. How much leakage the parallel paths may have is a critical question to address in order to design APAM device for RT operation. TCAD device modeling can be very useful to help answer this question.

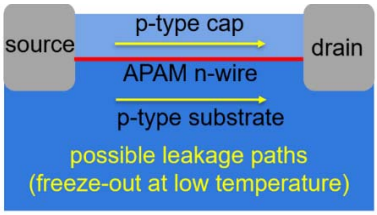

Fig. 1. Schematic of APAM wire device with leakage paths denoted by yellow lines. Leakage paths through cap layer and substrate are freeze-out at 4 Kelvin but become important at RT.

II. Applicability of Semiclassical Simulation

To assess the applicability of semiclassical TCAD simulation to APAM devices, we first modeled electron mobility in a highly doped semiconductor using semiclassical scattering theory; then we simulated APAM wire sheet resistance using semiclassical TCAD simulation and compared with experimental data.

Electron mobility extracted from Hall measurements of APAM n-type wires are known to have low values on the order of 50 to 100 $cm^2/(V.s)$ or less [5-8]. Hwang and Das Sarma [9] used a somewhat sophisticated two-dimensional (2D) treatment to model the electron mobility and achieved qualitative agreement with measured data. Nonetheless, we will show that by using the simple, semiclassical, 3D ionized impurity scattering theory, we can obtain electron mobility values that are not only qualitatively consistent with measured data, but also can reproduce the data with a single parameter.

This work is funded under Laboratory Directed Research and Development Grand Challenge (LDRD GC) program, Project No. 213017, at Sandia National Laboratories. Sandia National Laboratories is a multimission laboratory managed and operated by National Technology and Engineering Solutions of Sandia, LLC., a wholly owned subsidiary of Honeywell International, Inc., for the U.S. Department of Energy's National Nuclear Security Administration under contract DE-NA-0003525.

This paper describes objective technical results and analysis. Any subjective views or opinions that might be expressed in the paper do not necessarily represent the views of the U.S. Department of Energy or the United States Government.

We started with the famous mobility Drude model [10], i.e., $\mu = q\langle\langle\tau_m\rangle\rangle/m_c^*$, where $\langle\langle\tau_m\rangle\rangle$ denotes a specially defined averaged momentum relaxation time, m_c^* is the conductivity effective mass [11]. The momentum relaxation time τ_m is

$$\frac{1}{\tau_m} = \sum_{\vec{k}'} S(\vec{k},\vec{k}')\left(1-\frac{\vec{k}'\cdot\vec{k}}{k^2}\right)\left(1-f(\vec{k}')\right), \qquad (1)$$

where $f(\vec{k}')$ is the probability that the state at $\vec{k}'$ is occupied. The transition rate from an initial wave vector $\vec{k}$ to a final $\vec{k}'$ can be computed using the Fermi's Golden Rule as

$$S(\vec{k},\vec{k}') = \frac{2\pi}{\hbar}\left|\langle\psi_{\vec{k}'}|\hat{H}_{int}|\psi_{\vec{k}}\rangle\right|^2\delta\left[E(\vec{k}')-E(\vec{k})\right], \qquad (2)$$

where the $\delta[.]$ term ensures energy conservation. The interaction Hamiltonian depends on the scattering type.

Due to the high doping in APAM devices, electron mobility is limited by ionized impurity scattering especially at low temperatures. Hence, we focus on the ionized impurity scattering only. By solving the Poisson equation for a n-type semiconductor, we obtain the screened electron-impurity interaction Hamiltonian as $\hat{H}_{int} = q^2e^{-r/L_D}/(4\pi\varepsilon_0\varepsilon_s r)$, with L_D being the Debye length [10] and q being the elemental charge. L_D is given by $L_D = \sqrt{\varepsilon_0\varepsilon_s k_B T/(q^2 n\alpha)}$, where T is the lattice temperature and n is the electron density. Depending on the carrier statistics used in expressing the electron density when solving the Poisson equation, we obtain either $\alpha = 1$ for Boltzmann statistics, or $\alpha = \mathcal{F}_{-1/2}(\eta_F)/\mathcal{F}_{1/2}(\eta_F)$ for Fermi-Dirac (FD) statistics. $\mathcal{F}_l(\eta_F)$ is the Fermi-Dirac integral of the lth order [12], and $\eta_F = \mathcal{F}_{1/2}^{-1}(n/N_C)$, the inverse of the FD integral of the 1/2 order, with N_C being the conduction band effective density of states.

Assuming parabolic conduction band, empty final state (i.e., $1-f(\vec{k}') \approx 1$), and weak energy dependence, we obtain the electron mobility due to impurity scattering as [10]

$$\mu = \frac{q}{m_c^*}\frac{128\sqrt{2\pi m_{dos}^*}\varepsilon_0^2\varepsilon_s^2(k_BT)^{3/2}}{q^4N_d\left[\ln(1+\gamma^2)-\frac{\gamma^2}{1+\gamma^2}\right]}, \quad \gamma = \frac{2L_D}{\hbar}\sqrt{6k_BTm_{dos}^*}. \qquad (3)$$

Here m_{dos}^* is the density-of-states effective mass, N_d is the doping density, ε_s is the static dielectric constant. To compute the electron mobility as a function of doping density and temperature, we assume $n = N_d$ and use the effective masses of bulk silicon [11], i.e., $m_{dos}^* = 1.08m_0$ and $m_c^* = 0.26m_0$. For the FD case, we also need to know the temperature dependence of N_C. For parabolic conduction band in silicon, $N_C(T)$ is given by

$$N_C(T) = 2.51\times10^{19}\left(\frac{m_{dos}^*}{m_0}\frac{T}{300}\right)^{\beta} = 2.82\times10^{19}\left(\frac{T}{300}\right)^{\beta}, \qquad (4)$$

where the second equal sign assumes m_{dos}^* is independent of temperature. For silicon, $\beta = 1.5$ is often assumed. The electron mobility due to ionized impurity scattering in silicon is plotted in Fig. 2 as a function of the donor density at three different temperatures. Clearly, in the low doping regime, both Boltzmann and FD statistics produce the same mobility, and the mobility is higher for higher temperature since hot electrons are less likely scattered by impurities. As the doping density increases, the Boltzmann assumption becomes invalid, which happens at lower density for lower temperature.

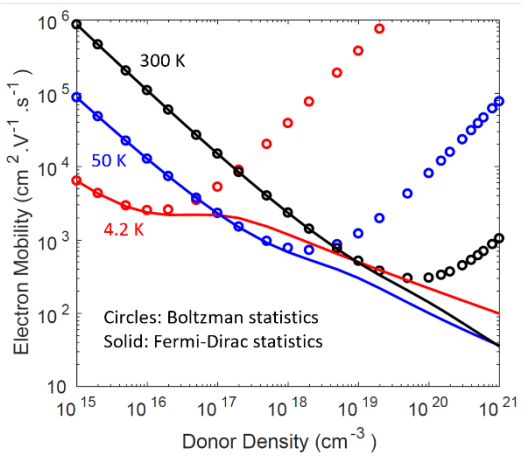

Fig. 2. Calculated electron mobility vs. donor density at three temperatures. The circles were obtained using the Boltzmann statistics in computing L_D (with $\alpha = 1$), while the solid lines were obtained using the FD statistics. The results were generated using β = 1.5 in computing $N_C(T)$.

It is noted that in the high doping regime, the electron mobility due to ionized impurity scattering alone indeed becomes small, on the order of 100 cm^2/(V.s). Also note that the described mobility model is based on the 3D impurity scattering theory that is much simpler than the 2D model by Hwang [9]. A natural question is how the mobility values produced by this 3D scattering model compare with experimental data. In Fig. 3, we plotted the calculated mobility at high doping using three β values and compared with measured mobility in the literature. We found that by varying the β value slightly, the computed mobility values can reproduce the measured data surprisingly well. The variation of β value could be because the effective mass is temperature dependent [13].

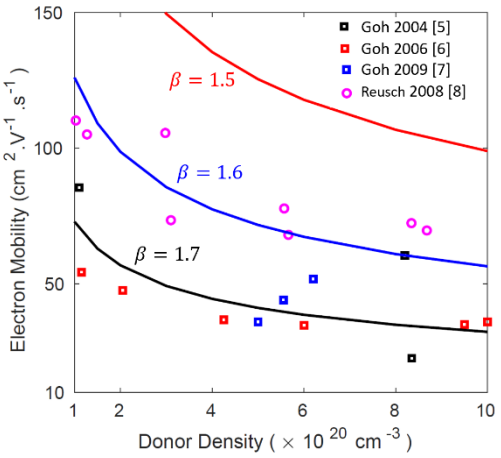

Fig. 3. Comparison of calculated electron mobility (solid lines) with experimentally extracted mobility (symbols) at 4 K. β is the exponent in (4). For comparison, the sheet doping density in experimental data was converted to 3D density assuming a 2-nm thickness.

To further evaluate semiclassical TCAD applicability to APAM devices, we simulated a simplified APAM wire shown in the inset of Fig. 4, using Sandia's open-source TCAD code, Charon [14-15], which is a 2D/3D, MPI-parallel, device simulation tool. The simulated sheet resistance versus the delta-layer doping density is shown in Fig. 4 and compared with cryogenic measurements by Goh et al. [6]. For comparison, the sheet doping density in Goh's paper was converted to 3D doping density assuming a 2-nanometer (nm) thick delta-layer as used in Charon's simulation. It is seen that,

by using the extracted mobility values from [6], Charon reproduces the sheet resistance vs. doping density well when compared to the experimental data. The curves also follow the classical sheet resistance vs. doping density well, i.e., $R_s = 1/qN_d\mu_n t$, with t being the delta-layer thickness.

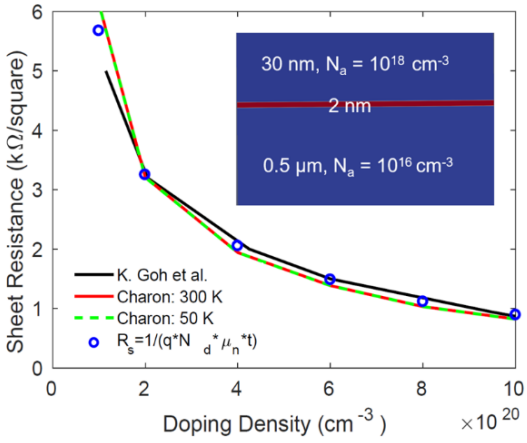

Fig. 4. Simulated sheet resistance vs. delta-layer doping density and comparison with measured data by Goh et al. [6]. Note that Charon results have no temperature dependence because a constant mobility at a given doping density was used. Inset: simulated APAM wire with contacts connecting the left and right edges of the red delta-layer.

From the above study, we see that the very low mobility in APAM wires can be explained using a simple 3D ionized impurity scattering model with the FD statistics. Furthermore, fast semiclassical TCAD simulation can reproduce sheet resistances of APAM wires, when proper electron mobility values are used, which can be obtained from either Hall measurements or a simple mobility model. While detailed quantum transport modeling may be intuitively more appropriate for cryogenic measurements, or given the tight confinement of electrons within the phosphorus layer, the above work indicates that semiclassical TCAD simulation provides a straightforward path to empirical understanding of APAM devices. In the following, we will apply semiclassical TCAD to realistic APAM devices to model current leakage and improve APAM device design for RT operation.

III. Modeling Assisted APAM RT Device Design

To design a structure to overcome the limitations of the device in Fig. 1, we apply Charon to model the current leakage through the p-type cap layer. The goal is to figure out what cap doping and thickness are needed to minimize leakage through the cap at RT. The simulated 2D structure is shown in Fig. 5, which represents a cross section of an APAM wire. Simulation results show hole current leakage in the cap layer is a trade-off between p-doping density and layer thickness. The current leakage for different cap doping and thickness is summarized in Fig. 6, where the leakage increases with increasing doping density and increasing thickness. The reason is that at a given thickness, the depletion width in the cap is smaller for a higher cap doping, and consequently more un-depleted holes lead to current leakage. For 10^{18}-cm^{-3} doping and 30-nm layer, the leakage is negligible because the cap is fully depleted at this condition. This result is also consistent with the PN junction depletion approximation, i.e., the depletion width, $W = \sqrt{2\varepsilon_0\varepsilon_s(N_d + N_a)V_{bi}/qN_dN_a} \approx 38$ nm for $N_d = 4 \times 10^{20}$ and $N_a = 10^{18}$ cm-3, which is comparable to the 30-nm layer thickness.

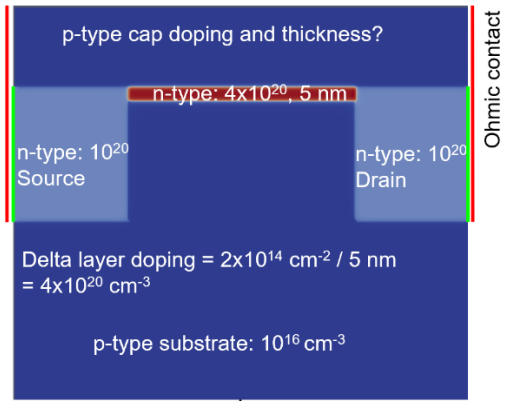

Fig. 5. Simulated 2D structure representing cross section of an APAM wire, where the delta-doped layer is approximated by a 5-nm doped region. Current leakage is simulated using the current difference between contacting and not contacting the cap layer.

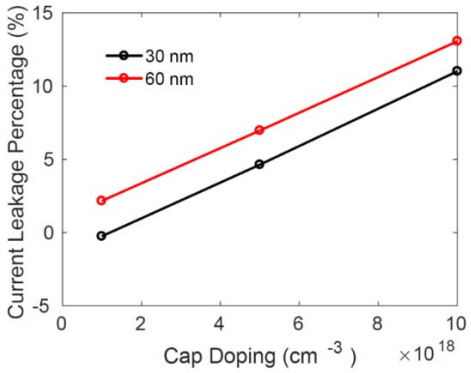

Fig. 6. Simulated current leakage as a function of the cap doping for cap layer thickness of 30 and 60 nm.

From the above study, we learned that by choosing appropriate doping and thickness for the cap layer, we could minimize the cap leakage. While depletion of the holes in the cap can suppress the leakage through the cap, additional care must be taken to suppress the leakage channel through the substrate. Therefore, we also isolate the contact regions from the cap and substrate regions using field oxide to further reduce possible hole leakage at RT. Fig. 7 shows a cross-section schematic of the modeling assisted new device design towards RT operation.

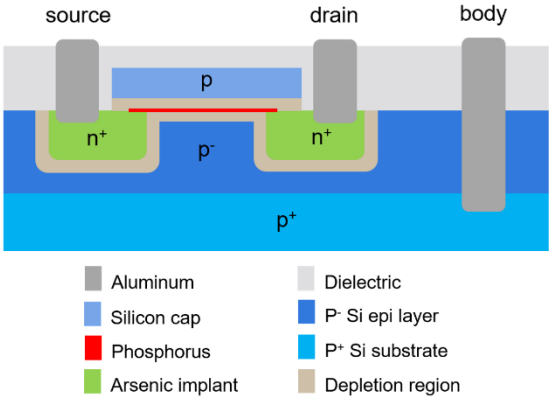

Fig. 7. Cross-section schematic of the modeling assisted new device design for RT operation. The red line denotes an APAM n-type wire. The wire contacts are isolated from the cap and substrate regions by field oxide.

Based on the device design in Fig. 7, we have fabricated Hall bar devices with and without the STM-doped delta layer.

A top view of the Hall bar is given in Fig. 8. Without the delta layer, the measured resistance at RT between the source and drain contacts (i.e., between contacts 4 and 8 in Fig. 8) is on the order of 300 MΩ, suggesting current leakage via the cap and substrate regions is minimal. With the delta layer, the measured wire resistance at RT is about 27 kΩ, close to the value of a similar APAM wire measured at 4 K. The delta-layer sheet electron density is calculated to be about $8x10^{13}$ cm^{-2} from four-probe measurement. This result also agrees with RT infrared measurements of the optical conductivity [16] of a similar APAM wire.

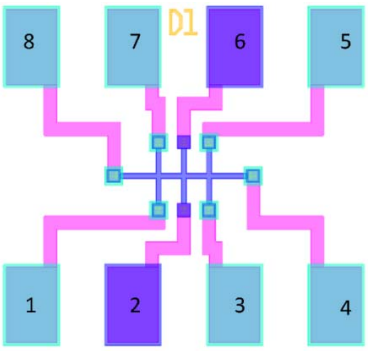

Fig. 8. Top view of APAM Hall bar where the main wire is between contacts 4 and 8 indicated by the purple line. The wire is 500-µm long and 20-µm wide.

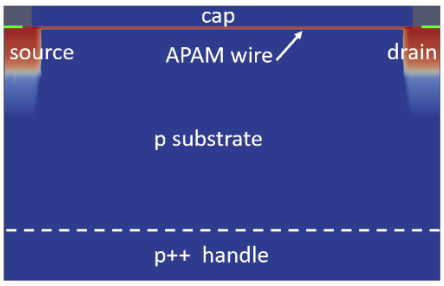

Fig. 9. Simulated 2D structure representing a 2-µm-long cross section of the RT Hall bar. The green solid lines indicate the source and drain Ohmic contacts. The isolation oxide between the cap and the Ohmic contacts is not included in the simulation since it does not affect current flow

To correlate simulation with experiment, we set up a simulation structure shown in Fig. 9. The APAM wire is 4-nm thick and its doping was set to $2x10^{20}$ cm^{-3} based on the measured sheet density of $8x10^{13}$ cm^{-2}. Doping profiles from secondary ion mass spectrometry (SIMS) of similar samples were used in the source/drain and substrate regions. The cap layer thickness and doping in similar samples can vary significantly due to unintentional variation in the STM process. For simulation purpose, the thickness of the cap layer was set to a designed value of 30 nm, while the cap doping was assumed to be a nominal value of $5x10^{18}$ cm^{-3}. Simulation was done using Charon [14]. Standard silicon models and parameters were used, e.g., the Slotboom model [17] for band gap narrowing, Shockley-Read-Hall (SRH) recombination, Fermi-Dirac statistics for high doping, and the Arora model [18] for carrier mobility. It turned out that the electron mobility computed using the Arora model is about 90 $cm^2/(V.s)$ in the APAM wire, which is in the measured mobility range shown in Fig. 3. The simulated resistance is 105 Ω for the 2-µm-long wire, leading to an extrapolated value of 26 kΩ for the fabricated 500-µm-long wire. Without any calibration, the simulated resistance agrees surprisingly well with the measured data. There was some uncertainty in the cap doping level in the fabricated device. However, our simulation results showed that, even for a range of two orders of magnitude difference in the cap doping, the simulated wire resistance was still on par with the measured value. This confirms that the current at RT is indeed mainly carried by the APAM wire and other leakage path is negligible.

IV. Conclusions

We have shown that the carrier transport in APAM devices can be modeled by semiclassical transport theory, especially at elevated temperatures, despite the nominally atomic monolayer doping. We showed that semiclassical TCAD simulation provided fast and instrumental insight to design APAM device for RT operation. With input from TCAD modeling, we have demonstrated RT operation of an APAM wire device for the very first time, which paves the path toward APAM enabled transistor for microelectronics.

References

[1] F. J. Ruess, L. Oberbeck, M. Y. Simmons, K. E. J. Goh, A. R. Hamilton, T. Hallam, et al., "Toward atomic-scale device fabrication in silicon using scanning probe microscopy," Nano Letters, vol. 4, no. 10, pp. 1969–1973, 2004.

[2] D. R. Ward, S. W. Schmucker, E. M. Anderson, E. Bussmann, L. Tracy, T. Lu, et al., "Atomic precision advanced manufacturing for digital electronics," Elec. Dev. Fail. Anal. vol 22, pp. 4-10, 2020.

[3] Y. He, S. K. Gorman, D. Keith, L. Kranz, J. G. Keizer, and M. Y. Simmons, "A two-qubit gate between phosphorus donor electrons in silicon," Nature, vol. 571, pp. 371-375, 2019.

[4] D. Mamaluy, J. P. Mendez, X. Gao, and S. Misra, "Open-system quantum treatment of Si:P delta-layers and implications," unpublished.

[5] K. E. J. Goh, L. Oberbeck, M. Y. Simmons, A. R. Hamilton, and R. G. Clark, "Effect of encapsulation temperature on Si:P δ-doped layers," Appl. Phys. Lett., vol. 85, no. 21, pp. 4953-4955, 2004.

[6] K. E. J. Goh, L. Oberbeck, M. Y. Simmons, A. R. Hamilton, and M. J. Butcher, "Influence of doping density on electronic transport in degenerate Si:P δ-doped layers," Phys. Rev. B, vol. 73, 035401, 2006.

[7] K. E. J. Goh and M. Y. Simmons, "Impact of Si growth rate on coherent electron transport in Si:P δ-doped devices," Appl. Phys. Lett., vol. 95, art. 142104, 2009.

[8] T. C. G. Reusch, K. E. J. Goh, W. Pok, W.-C. N. Lo, S. R. McKibbin, and M. Y. Simmons, "Morphology and electrical conduction of Si:P δ-doped layers on vicinal Si(001)," J. of Appl. Phys., vol. 104, art. 066104, 2008.

[9] E. H. Hwang and S. Das Sarma, "Electronic transport in two-dimensional Si:P -doped layers," Phys. Rev. B, vol. 87, art. 125411, 2013.

[10] M. Lundstrom, Fundamentals of Carrier Transport, 2nd ed., Cambridge University Press, 2000.

[11] M. Lundstrom, "Notes on effective mass," nanohub.org, 2013.

[12] R. Kim and M. Lundstrom, "Notes on Fermi-Dirac integrals," 3rd ed., arXiv:0811.0116, August 2011.

[13] D. M. Riffe, "Temperature dependence of silicon carrier effective masses with application to femtosecond reflectivity measurements," J. Opt. Soc. Am. B, vol. 19, no. 5, pp. 1092-1100, 2002.

[14] https://charon.sandia.gov/.

[15] X. Gao, B. Kerr, and A. Huang, "Analytic band-to-trap tunneling model including band offset for heterojunction devices," J. Appl. Phys., vol. 125, art. 054503, 2019.

[16] A. Katzenmeyer, T. S. Luk, E. Bussmann, S. Young, E. Anderson, M. Marshall, et al., "Assessing atomically thin delta-doping of silicon using mid-infrared ellipsometry," J. Mat. Res., pp. 1-8, June 2020.

[17] J. W. Slotboom, "The pn production in silicon," Solid-State Electron., vol. 20, pp. 279-283, 1977.

[18] N. D. Arora, J. R. Hauser, D. J. Roulston, "Electron and hole mobilities in silicon as a function of concentration and temperature," IEEE. Trans. Electron Devices, vol. 29, no. 2, pp. 292-295, 1982.